Characterization of High Enthalpy Facilities and Streamlining of Calibration and Tests (CHEF)

Technical Note 5

Task 7:

Uncertainty Assessment on Experimental Data

Ana Isabel del Val Benítez, Thierry Magin, Olivier Chazot

von Karman Institute for Fluid Dynamics
Aeronautics and Aerospace Department

13/11/2016

Contents

Nomenclature

Latin Symbols

Da	Damköhler number
e	specific energy, J/kg
E	total energy, J/kg
h	specific enthalpy, J/kg
J	Jacobian matrix
k_B	Boltzmann constant, J/K
$\dot{m}$	mass flow, kg/s
Le	Lewis number
M	Mach number
Nu	Nusselt number
p	pressure, Pa
P_w	electrical power, W
Pr	Prandtl number
q	heat flux, W/m^2
R	matrix of residuals
Re	Reynolds number
R_{eff}	effective radius, m
s	specific entropy, J/kgK
S	cross-sectional area, m^2
T	temperature, K
T_{ref}	temperature of reference, K
U	matrix of unknowns in a Newton method
v	velocity, m/s
V	diffusion velocity, m/s
x	mole fraction
y	mass fraction

Greek Symbols

β	velocity gradient, s^{-1}
Δ	gradient operator
γ	specific heat ratio
λ	thermal conductivity, W/m.K
μ	dynamic viscosity, Pa.s
ρ	density, kg/m^3
τ	characteristic time, s

Subscripts/Superscripts

D	dissociation
i	gas species
NS	number of species
R	reactive
s	stagnation magnitude
t_2	stagnation conditions after the shock
w	at the wall
0	stagnation conditions in the reservoir
1	pre-shock conditions
2	post-shock conditions
∞	free-stream value

Abbreviations

DLR	Deutsches Zentrum für Luft- und Raumfahrt
ICP	Inductively-Coupled Plasma
LTE	Local Thermodynamic Equilibrium
OES	Optical Emission Spectroscopy
TPS	Thermal Protection System
VKI	von Karman Institute

1 Introduction

The rebuilding of the free stream parameters in the LBK arc-jet facility is not exempt of associated uncertainties representing the object of this study. The **C**onserv**A**tion **B**alance equation code for **A**tmosphe**R**ic **E**n**T**ry, **CABARET**, is the rebuilding code that will be used here. This rebuilding methodology is based on a forward problem followed by a Newton-Raphson iterative method in order to invert the problem and compute the quantities needed.

From the experimental data of the different cases in the CHEF project, a few rebuilding scenarios can be adopted according to the set of inputs used. The advantages of having different sets of measurements available for rebuilding procedures lay on the fact that these measurements do not have the same experimental uncertainties which is directly link with the accuracy of the rebuilding.

In the following section, the theory behind CABARET is exposed together with the numerical scheme used for the iterative process. The results of sensitivity analysis and uncertainty quantification based on Monte Carlo random sampling are presented in section 3. Relevant conclusions extracted from this work are explained in section 4.

2 Rebuilding procedure

2.1 Overview and flowchart

In this section, the numerical tool developed to perform the rebuilding of the free stream conditions in high enthalpy facilities will be described. The computation of the free stream flow properties in high enthalpy facilities and plasma wind tunnels such as the LBK arc-jet (Gülhan and Esser (2002)) and VKI Plasmatron (Bottin et al. (1999)), can be achieved by using the VKI Mutation++ library developed by Scoggins (2014) and different experimental inputs as seen in Table 1 (used in sets of three).

Mass flow rate [g/s]	$\dot{m}$
Reservoir pressure [hPa]	p_0
Reservoir temperature [K]	T_0
Stagnation pressure [hPa]	p_{t2}
Heat flux [MW/m^2]	q_w

Table 1: Experimental data used for different rebuildings

In this report, three measurements have been taken into account to serve as an example of how the rebuilding code works. These measurements are namely the stagnation point heat flux q_w, the stagnation point pressure p_{t2} and the reservoir pressure p_0 which are the standard ones used in other high enthalpy facilities. The exact procedure followed is illustrated in Figs. 1 and 2 to which the reader is referred to for each of the steps described hereafter.
The test gas used in the facilities is air. A mixture of 13 species ($N, N+, O, O+, NO, N_2$ $N_2+, O_2, O_2+, NO+, e-, Ar, Ar+$) is taken into account by the Mutation++ library for the rebuilding procedure. The mixture used can be adapted to different facilities and tests, in this case, argon has been taken into account for this particular facility.

The aim is to find the unknown free-stream quantities (the temperature T_∞, the static pressure p_∞ and the velocity v_∞) which provide a satisfactory set of free-stream conditions to match the measured stagnation point heat flux q_w on a hemispherical probe, the stagnation point pressure p_{t2} and the reservoir pressure p_0 . Conservation equations across a normal shock wave are solved during the procedure.

2.2 Measurements required

The measurements required for performing the rebuilding by applying this method are the stagnation point heat flux q_w, the stagnation point pressure p_{t2} and the reservoir pressure p_0. This measurements are performed by intrusive measurement techniques such as immersing calorimeters and Pitot probes in the flow. Other type of measurements are the Optical Emission Spectroscopy (OES) (Le Quang. (2014)) that can measure free stream values and are mainly used when the tests are carried out without probe to characterize the free stream.

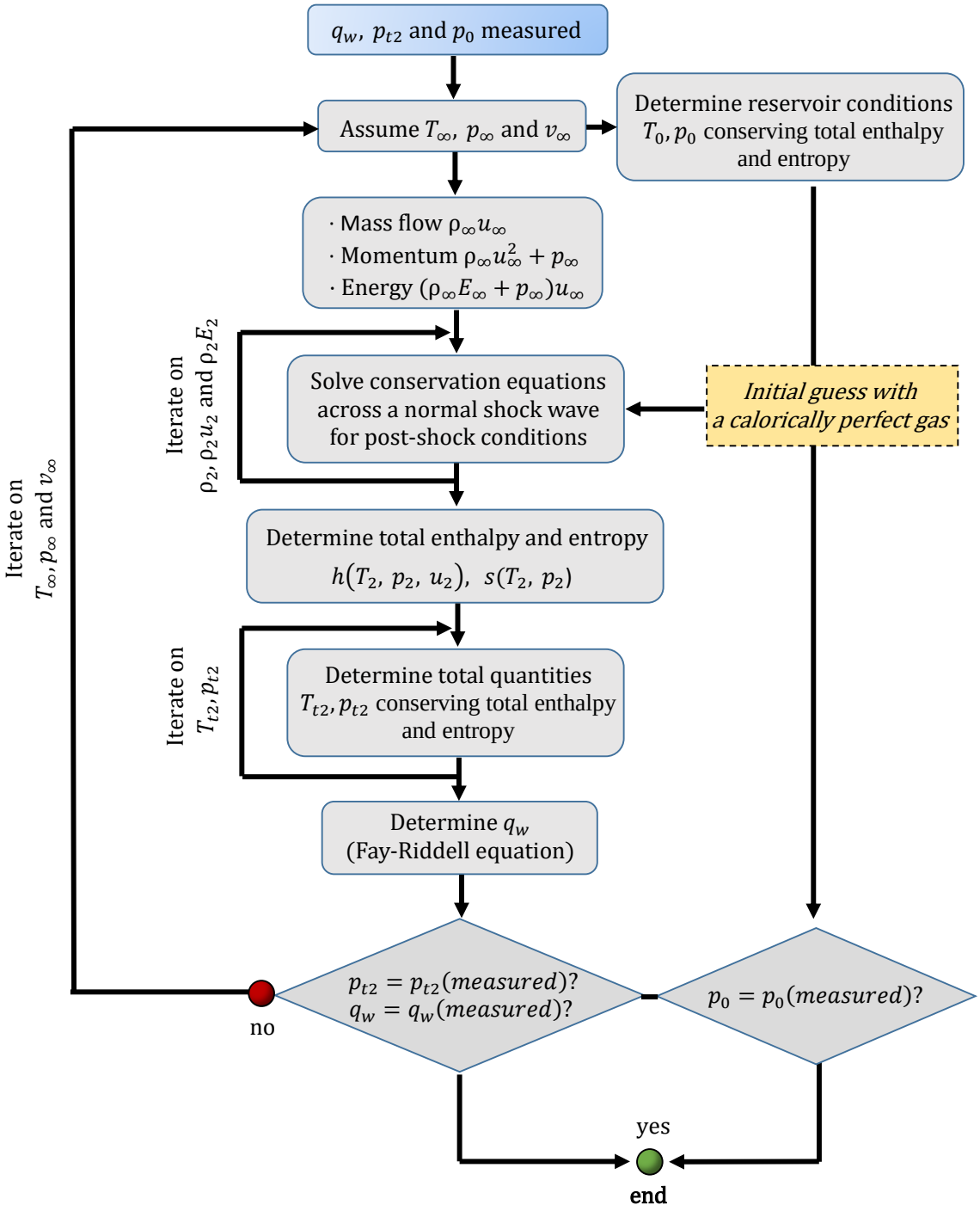

Figure 1: Flowchart of the rebuilding method

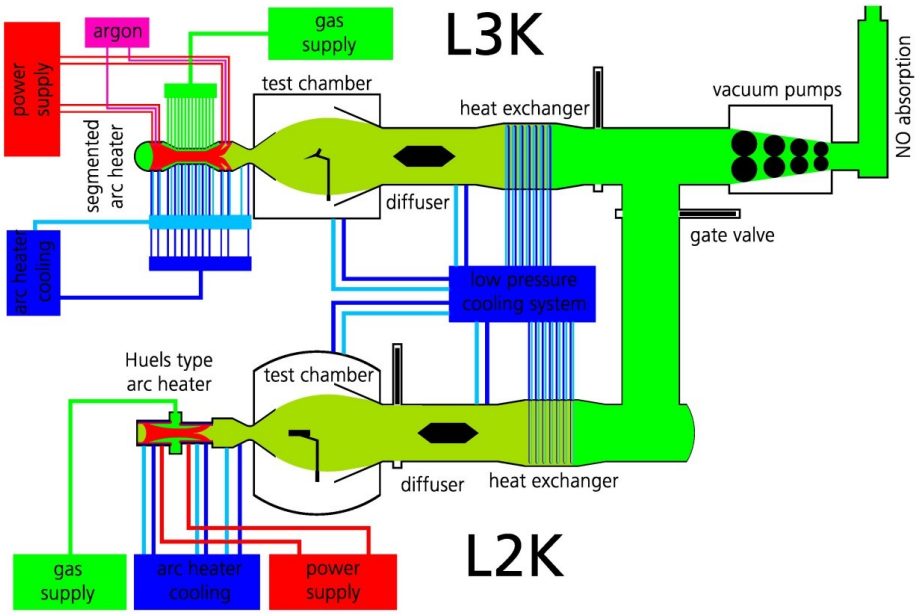

Figure 2: DLR's LBK (L2K and L3K) facility

2.3 Assumptions

The assumptions used to determine the free stream flow properties are relatively limited. A description of the nozzle flow behavior during the expansion, i.e. the commonly used adiabatic and isentropic flow expansion assumptions are needed.
The assumptions regarding equilibrium in the flow, the computation of thermodynamic and transport properties together with the heat flux equation will be explained hereafter.

2.3.1 Local Thermodynamic Equilibrium

One of the main assumptions is to consider the plasma to be in Local Thermodynamic Equilibrium (LTE).
The plasma, composed of a gas mixture of various species, adapts its composition instantaneously to changes in the flow so it can be thought as a single gas with a determined composition or a gas in **chemical equilibrium** (see Van Der Haegen (2013)).

In the context of **thermal equilibrium**, the temperature and the pressure are enough to define the distribution of species and a single temperature can be used to describe the flow which does not depend on its history.

When the flow is in thermal and chemical equilibrium it is said to be in local thermodynamic equilibrium, this is equivalent to say that de Damköhler number tends to infinite

$$Da = \frac{\tau_{flow}}{\tau_{chemical}} \rightarrow \infty \tag{1}$$

With τ being, respectively, the characteristic time of the flow (τ_{flow}) and the one of the chemical reactions ($\tau_{chemical}$).

2.3.2 Thermodynamic and transport properties

The use of the Mutation++ library provides the new numerical code with accurate transport and thermodynamic properties for ionized gases. The thermodynamic properties needed are the enthalpy and entropy of a gas mixture shown in Eqs. 2-3, respectively:

$$h = \sum_{i=1}^{NS} y_i(p, T, x_j) h_i(T) \tag{2}$$

$$\rho s = \sum_{i=1}^{NS} \rho_i s_i + k_B \tag{3}$$

In the case of the entropy there is an extra term compared with the equivalent equation for the enthalpy. This term is the entropy of mixing. In these equations, y_i stands for the mass fraction of species i, while x_i is the mole fraction. The term k_B is the Boltzmann's constant, also in these equations, h_i and s_i are the enthalpy and entropy of the species i, respectively.

Regarding the transport properties, they are computed through a multiscale Chapman-Enskog perturbative solution of the Boltzmann equation:

- **Dynamic viscosity**

The dynamic viscosity is obtained from the first and second Laguerre-Sonine polynomial approximations respectively of the Chapman-Enskog expansion. The resulting expression requires the solution of the linear transport systems:

$$\sum_{j=1}^{NS} G_{ij}^{\mu} \alpha_j^{\mu} = x_i \tag{4}$$

$$\mu = \sum_{i=1}^{NS} \alpha_i^{\mu} x_i \tag{5}$$

where μ and G^{μ} are transport matrices depending on the species mole fractions and binary collision integrals. Fig. 3 shows the variation of the dynamic viscosity, μ, with the temperature for different pressure cases

As can be appreciated in Fig. 3, the dynamic viscosity presents a maximum at nearly 7000 K, after that, it decreases due to the rarefication of the gas and the consequent increasing of the particles cross section.

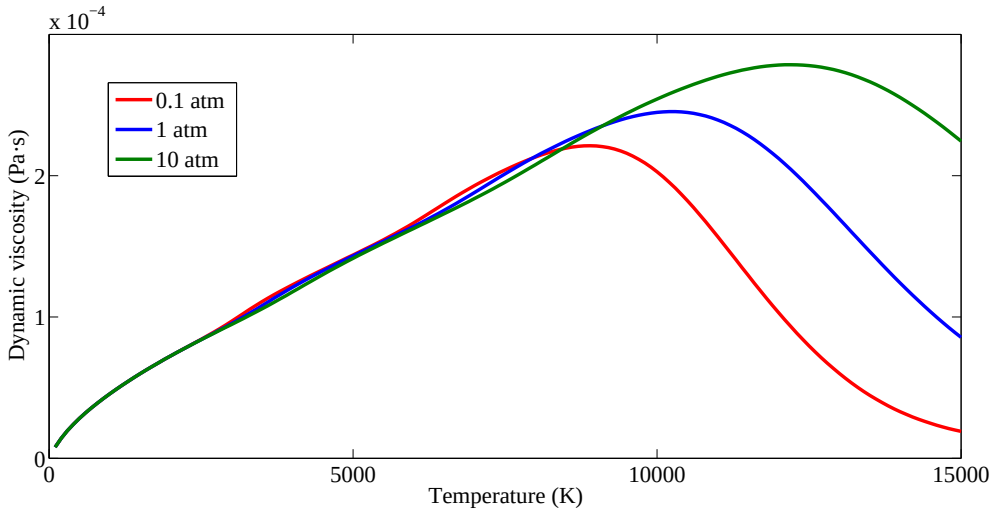

Figure 3: Dynamic viscosity computed with Mutation++ for 0.1, 1 and 10 atm

- **Thermal conductivity**

The general equation of heat flux considers convective and diffusive terms:

$$q = -\lambda \nabla T + \sum_{i=1}^{NS} \rho_i V_i h_i \tag{6}$$

Using Fick's law:

$$\rho_i V_i = -\sum_j D_{ij} \nabla x_j, \;\; \nabla x_j = \frac{\partial x_j}{\partial T} \nabla T \tag{7}$$

Eq. 6 can be rewritten as:

$$q = -(\lambda + \lambda^R) \nabla T \tag{8}$$

where

$$\lambda^R = \sum_{i,j} h_i(T) D_{ij} \frac{\partial x_j}{\partial T} \tag{9}$$

Eq. 8 is the equivalent form of the convective term but also considering the diffusive part. In general, thermal conductivity is computed in Mutation++ as:

$$\sum_{i=1}^{NS} G_{ij}^{\lambda} \alpha_j^{\lambda} = x_i \tag{10}$$

$$\lambda = \sum_{j=1}^{NS} \alpha_j^{\lambda} x_j \tag{11}$$

All the details behind the modeling of these properties are explained by Scoggins (2014).

2.3.3 Heat flux equation

The Fay and Riddell (1958) equation is used to relate free stream conditions to the stagnation point heat flux. This might be the most severe assumption and currently restricts the test gas to air (or nitrogen) for which it was developed. Ideally, this should be replaced by a numerical code able to predict the stagnation point heat flux accurately for a wide variety of free-stream compositions and conditions.

2.4 Theoretical frame: detailed procedure

2.4.1 Shock wave relations

The free stream is found to be at high Mach number regime on ground facilities (supersonic and hypersonic) so in order to adapt the flow to the model wall conditions, a detached shock wave appears in front of the model. This shock wave is analyzed locally in the stagnation region as a normal shock wave.

The approach used to compute the flow parameters behind the shock wave is the Rankine-Hugoniot set of equations. These equations are the inviscid flow equations applied in a finite volume in which the shock wave is contained. The jump in the flow parameters through the shock wave is then governed by the conservation of mass, momentum and energy, respectively:

$$\rho_1 v_1 = \rho_2 v_2 \tag{12}$$

$$p_1 + \rho_1 v_1^2 = p_2 + \rho_2 v_2^2 \tag{13}$$

$$(\rho_1 E_1 + p_1) v_1 = (\rho_2 E_2 + p_2) v_2 \tag{14}$$

Where the total energy appeared in Eq. 14 follows the expression:

$$E = e + \frac{1}{2} v^2 \tag{15}$$

The sub indexes 1 and 2 denote the pre and post-shock conditions, respectively, being the pre-shock conditions the corresponding to the free stream conditions in this problem.

In these expressions, only the inviscid condition is imposed in the Navier-Stokes equations so the general character of the equations regarding equilibrium or non-equilibrium condition is conserved and represents an advantage in the case of non-equilibrium which can be considered for other facilities in the future.

The terms regarding the internal energy and the density have been calculated using the Mutation++ library.
As it could be appreciated before, the Rankine-Hugoniot relations are non-linear and need to be solved through an iterative method, such as the Newton-Raphson method. An initial approximate solution to this system is provided by assuming $\gamma = 1.4$ in both regions upstream and downstream of the shock, and using $M_1 = v_1/\sqrt{\gamma R T_1}$. The static pressure, temperature, density and velocity after a normal shock are expressed for such a calorically perfect gas by

eqs. 16 to 19.

$$p_2 = p_1 \frac{2\gamma M_1^2 - (\gamma - 1)}{\gamma + 1} \tag{16}$$

$$T_2 = T_1 \frac{[2\gamma M_1^2 - (\gamma - 1)][(\gamma - 1)M_1^2 + 2]}{(\gamma + 1)^2 M_1^2} \tag{17}$$

$$\rho_2 = \rho_1 \frac{(\gamma + 1)M_1^2}{(\gamma - 1)M_1^2 + 2} \tag{18}$$

$$v_2 = v_1 \frac{(\gamma - 1)M_1^2 + 2}{(\gamma + 1)M_1^2} \tag{19}$$

It is also important to take into account the reference frame in which the velocity before and after the shock wave is considered. In this case, on the ground testing facilities the shock wave is attached and presents no movement in relation to an absolute axis referred to the ground so it is assumed that $u_s = 0$ which is different from the flight condition in which the shock wave is moving so $u_s \neq 0$.

Equations 12 to 14 are then solved based on the initial guesses described before for a calorically imperfect gas using a Newton method. Unknowns of the system are expressed by the matrix U as:

$$U = \begin{bmatrix} \rho_2 \\ \rho_2 v_2 \\ \rho_2 E_2 \end{bmatrix} \tag{20}$$

The Newton method is written as $J\Delta U = -R$ where J is the Jacobian (eq. 21), U are the unknowns of the system (eq. 20) and the matrix R contains the residuals expressed by eq. 22.

$$J = \begin{bmatrix} \frac{\partial R_1}{\partial U_1} & \frac{\partial R_1}{\partial U_2} & \frac{\partial R_1}{\partial U_3} \\ \frac{\partial R_2}{\partial U_1} & \frac{\partial R_2}{\partial U_2} & \frac{\partial R_2}{\partial U_3} \\ \frac{\partial R_3}{\partial U_1} & \frac{\partial R_3}{\partial U_2} & \frac{\partial R_3}{\partial U_3} \end{bmatrix} \tag{21}$$

$$R = \begin{bmatrix} \rho_2 v_2 - \rho_1 v_1 \\ \rho_2 v_2^2 + p_2 - \rho_1 v_1^2 - p_1 \\ (\rho_2 E_2 + p_2) v_2 - (\rho_1 E_1 + p_1) v_1 \end{bmatrix} = \begin{bmatrix} [\rho u]_1^2 \\ [\rho u^2 + p]_1^2 \\ [(\rho E + p) u]_1^2 \end{bmatrix} \tag{22}$$

Iterations on the unknowns U are performed with eq. 23 (n designing the iteration index) until $|R| < \epsilon$ with $\epsilon > 0$. This ensures convergence of the post-shock flow properties to the desired degree of accuracy.

$$U^{n+1} = U^n - \frac{f(U^n)}{f'(U^n)} \tag{23}$$

Once these post-shock flow conditions are determined, other flow properties such as the enthalpy and the entropy of the test gas follow.

2.4.2 Total quantities

For computing the total quantities needed for solving the reservoir and also for computing the heat flux, the thermally perfect gas model is used. Differently from callorically perfect gas, thermally perfect gas does not have a constant specific heat ratio, γ. In Eqs. 16-17, the conservation of total enthalpy and entropy are used to compute the total quantities along the stagnation line:

$$h(T_t, p_t) = h(T, p) + \frac{v^2}{2} \tag{24}$$

$$s(T_t, p_t) = s(T, p) \tag{25}$$

These equations are applied to the post-shock conditions and are solved using the same method as described before for the shock relations.

$$U = \begin{bmatrix} p_{t2} \\ T_{t2} \end{bmatrix} \tag{26}$$

$$J = \begin{bmatrix} \dfrac{\partial R_1}{\partial p_{t2}} & \dfrac{\partial R_1}{\partial T_{t2}} \\ \dfrac{\partial R_2}{\partial p_{t2}} & \dfrac{\partial R_2}{\partial T_{t2}} \end{bmatrix} \tag{27}$$

$$R = \begin{bmatrix} h(T_{t2}, p_{t2}) - (h(T_2, p_2) + \frac{v_2^2}{2}) \\ s(T_{t2}, p_{t2}) - s(T_2, p_2) \end{bmatrix} \tag{28}$$

The total pressure p_{t2} will be compared later to experimental measurements. On the other hand, the total temperature T_{t2} is not easily measured practically and the measurement of the heat flux at the stagnation point of a hemispherical probe is preferred instead.

Another application of these conservation equations is for obtaining the conditions in the reservoir. Conservation of total enthalpy and entropy can be used along the stagnation line through the expansion in the nozzle in order to obtain the reservoir conditions from the free stream conditions by means of the same iterative process used for computing the post-shock conditions described before. In this case:

$$h(T_0, p_0) + \frac{v_0^2}{2} = h(T_1, p_1) + \frac{v_1^2}{2} \tag{29}$$

$$s(T_0, p_0) = s(T_1, p_1) \tag{30}$$

In Eqs. 29 and 30, the sub index 1 denotes the free stream parameters.
For closing the system, another additional equation is needed if the velocity in the reservoir is not supposed to be equal to zero, for this, the mass flow ($\dot{m}$) must be known:

$$\dot{m} = \rho_0(T_0, p_0) v_0 S_0 \tag{31}$$

In Eq. 31, the terms ρ_0, v_0 and S_0 are, respectively, the density and velocity of the flow in the reservoir, and its cross-sectional area. These three equations (29-31) are solved using the Newton method described before to obtain the reservoir conditions.

2.4.3 Stagnation point heat flux

The determination of the stagnation point heat flux is one of the most critical parts in the establishment of the theoretical frame. The heat flux calculation involves many different aspects of the flow and wall interaction which have to be taken into account in order to reach high accuracy levels that is translated into an efficient design of the Thermal Protection System. Some of these aspects come from the high enthalpy flow environment since the flow is mostly in thermo-chemical non-equilibrium.
For the purpose of this rebuilding problem, the well-known Fay-Riddell heat flux equation is used for equilibrium boundary layer conditions:

$$q_w = 0.763 Pr^{-0.6} (\rho_w \mu_w)^{0.1} (\rho_e \mu_e)^{0.4} (H_e - H_w) \sqrt{\beta_e} \left[1 + (Le^{0.52} - 1) \frac{h_D}{H_2} \right] \tag{32}$$

In Eq. 21 the e stands for *boundary layer edge* and the w stands for *model wall*. The Lewis number compares the molecular diffusion to thermal conduction and is taken equal to 1 (as suggested by Fay and Riddell). The Prandtl number compares viscous diffusion to thermal conduction and is normally set to the value 0.713, having:

$$q_w = 0.763 Pr^{-0.6} (\rho_w \mu_w)^{0.1} (\rho_e \mu_e)^{0.4} (H_e - H_w) \sqrt{\beta_e} \tag{33}$$

The nomenclature for the symbols and subscripts used is given in Fig. 4.

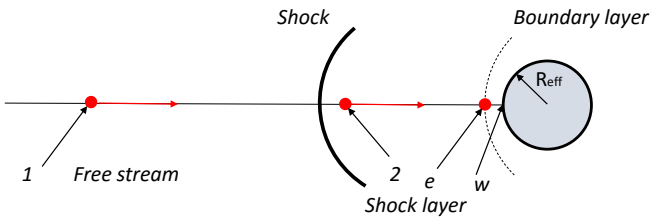

Figure 4: Nomenclature used by the Fay-Riddell equation

All the parameters regarding the flow properties such as the density, viscosity and enthalpy are computed using the Mutation++ library. The density at the wall ρ_w is computed from the stagnation point pressure p_{t2} (obtained previously) and the measured wall temperature T_w at the stagnation point while the density corresponding to the stagnation conditions is computed using both stagnation point pressure and temperature (p_{t2} and T_{t2}). The viscosity at the wall μ_w and the enthalpy H_w are also computed using the same temperature and pressure values (stagnation point pressure nad wall temperature) as inputs for the Mutation++ library as the enthalpy H_e and the viscosity μ_e are computed using the stagnation point conditions as explained before for the density.

The term β_e, the velocity gradient at the edge of the boundary layer, is taken as:

$$\beta_e = \frac{1}{R_{eff}} \sqrt{\frac{2(p_{t2} - p_1)}{\rho_{t2}}} \tag{34}$$

This expression results from the application of the Modified Newtonian Theory (MNT) that can be found in Anderson (2006).

2.4.4 Comparison to q_w, p_{t2} and p_0 measured and global iteration

The stagnation point pressure p_{t2}, the heat flux q_w and the reservoir pressure p_0 resulting from the initial choice of free stream conditions are finally compared to the experimental

values. Free stream unknowns T_∞, p_∞ and v_∞ (eq. 35) are iterated using a third Newton method (whose Jacobian is given by eq. 36) until the norm of the residuals R (eq. 37, the difference between the predictions and the measurements) is smaller than a prescribed value ϵ. Once convergence is achieved, the free stream, post-shock and stagnation point regions are all characterized.

$$U = \begin{bmatrix} T_\infty \\ p_\infty \\ v_\infty \end{bmatrix} \tag{35}$$

$$J = \begin{bmatrix} \dfrac{\partial q_w}{\partial T_\infty} & \dfrac{\partial q_w}{\partial p_\infty} & \dfrac{\partial q_w}{\partial v_\infty} \\ \dfrac{\partial p_{t2}}{\partial T_\infty} & \dfrac{\partial p_{t2}}{\partial p_\infty} & \dfrac{\partial p_{t2}}{\partial v_\infty} \\ \dfrac{\partial p_0}{\partial T_\infty} & \dfrac{\partial p_0}{\partial p_\infty} & \dfrac{\partial p_0}{\partial v_\infty} \end{bmatrix} \tag{36}$$

$$R = \begin{bmatrix} q_{w(predicted)} - q_{w(measured)} \\ p_{t2(predicted)} - p_{t2(measured)} \\ p_{0(predicted)} - p_{0(measured)} \end{bmatrix} \tag{37}$$

2.5 Limitations of the method

As a result of all the assumptions made along the way and explained in the previous sections, some other limitations have to be taken into account.

- Regarding the measurements of the Pitot pressure probe, some differences have to be considered when comparing the stagnation point pressure p_{t2} to the $P_{Pitot(measured)}$ due to viscous effects not taken into account in the formulation (Barker (1922)).
- Concerning the heat flux equation, Fay and Riddell obtained this expression not only analytically by studying the boundary layer but also by making correlations on the heat flux parameter ($Nu/\sqrt{Re}$) resulting from the boundary layer equations in order to obtain a unique equation for predicting the heat flux. This means that the equation has some limitations. Regarding the use of the equation in the rebuilding code, the quantities referred to the boundary layer edge are taken equal as the total quantities of the post-shock condition which is also an assumption that has to be validated.

3 Results and interpretation

In the following subsections, the experimental data provided for the three different free stream conditions (FC-I, FC-II and FC-III) are presented together with the associated uncertainties. A sensitivity analysis will be followed by an uncertainty quantification study for one of the free stream conditions (FC-II).

3.1 Experimental data and uncertainties

The experimental data used for the development of this work is presented in Tables 2-4.

Parameters	**Uncertainties**
Mass flow rate [g/s]: 101	±0.23%
Reservoir pressure [hPa]: 3800	±0.46%
Reservoir temperature [K]: 6550	±9.61%
Stagnation pressure [hPa]: 588	±1%
Heat flux (CTC) [MW/m^2]: 8	±10%

Table 2: Experimental data and uncertainties for condition FC-I

Parameters	**Uncertainties**
Mass flow rate [g/s]: 182	±0.32%
Reservoir pressure [hPa]: 5900	±0.82%
Reservoir temperature [K]: 5570	No data (±9.61%)
Stagnation pressure [hPa]: 1113	±1%
Heat flux (CTC) [MW/m^2]: 8.5	±10%

Table 3: Experimental data and uncertainties for condition FC-II

Parameters	**Uncertainties**
Mass flow rate [g/s]: 142	±0.0.27%
Reservoir pressure [hPa]: 5100	±0.6%
Reservoir temperature [K]: 5100	±15%
Stagnation pressure [hPa]: 85.4	±1%
Heat flux (CTC) [MW/m^2]: 1.24	±10%

Table 4: Experimental data and uncertainties for condition FC-III

3.2 Rebuilding scenarios

The versatility of the LBK facility in terms of the different measurements performed, allows us to rebuild the free stream conditions from three measurements picked among the experimental parameters presented in section 3.1. For the three testing conditions specified in the

framework of the CHEF project, the choice of experimental inputs together with the different rebuilding scenarios are exposed below. In Tables 5-7 different rebuilding scenarios have been taken into account to compute the free stream conditions under LTE assumptions for all three testing conditions.

N	**Scenario**	**Free stream temperature** [K]	**Free stream pressure** [Pa]	**Free stream Mach** [-]
1	q_w,P_{t2},P_0	3343.82	4367.89	3.3804
2	q_w,P_0,T_0	3477.32	3163.92	3.4771
3	P_{t2},P_0,T_0	3683.36	4463.64	3.2483
4	q_w,P_{t2},$\dot{m}$	3367.99	4452.27	3.34
5	q_w,T_0,$\dot{m}$	3483.44	3166.46	3.4709
6	q_w,P_0,$\dot{m}$	3513.7129	3010.89	3.4807
7	P_{t2},T_0,$\dot{m}$	3693.1065	4480.39	3.2403
8	P_{t2},P_0,$\dot{m}$	3774.08	4517.77	3.2149

Table 5: Rebuilding scenarios and rebuilt free stream parameters for condition FC-I

For the FC-II test conditions, the rebuilding results are more homogeneous due to the high heat flux, high pressure combination which has a better convergence for CABARET. The rebuilding results for the FC-II testing conditions are shown in Table 6:

N	**Scenario**	**Free stream temperature** [K]	**Free stream pressure** [Pa]	**Free stream Mach** [-]
1	q_w,P_{t2},P_0	3141.13	9556.89	3.18
2	q_w,P_0,T_0	3136.9	10255.81	3.14
3	P_{t2},P_0,T_0	3116.46	9614.16	3.17
4	q_w,$P_{t2}\dot{m}$	3138.94	9533.37	3.18
5	q_w,T_0,$\dot{m}$	3138.6	10269.35	3.13
6	q_w,P_0,$\dot{m}$	3138.79	9950.53	3.15
7	P_{t2},T_0,$\dot{m}$	3118.29	9631.67	3.16
8	P_{t2},P_0,$\dot{m}$	3127.05	9589.11	3.17

Table 6: Rebuilding scenarios and rebuilt free stream parameters for condition FC-II

Regarding the FC-III test conditions, problems arise when the heat flux is not high enough to consider the flow to be in supersonic operating conditions. In this case, the parameters rebuilt are not so accurate and a variability among the different scenarios can be appreciated.

N	**Scenario**	**Free stream temperature** [K]	**Free stream pressure** [Pa]	**Free stream Mach** [-]
1	q_w,P_{t2},P_0	975.84	232.36	5.31
2	q_w,P_0,T_0	1506.66	85.26	5.38
3	P_{t2},P_0,T_0	1963.56	315.96	4.61
4	q_w,$P_{t2}\dot{m}$	1115.26	272.5	4.91
5	q_w,T_0,$\dot{m}$	1618.78	91.43	5.19
6	q_w,P_0,$\dot{m}$	2080	39.08	5.76
7	P_{t2},T_0,$\dot{m}$	2117.27	359.22	4.49
8	P_{t2},P_0,$\dot{m}$	2547.78	332.97	4.8

Table 7: Rebuilding scenarios and rebuilt free stream parameters for condition FC-III

For conditions FC-I and FC-III there is enough data to be able to compare some flow parameters measured experimentally with the numerical code. Due to the LTE assumptions which lay behind CABARET, the measured free stream temperature is not comparable to the one rebuilt in the different cases but once the equilibrium is reached in the post-shock region, that is, when $T_v = T_{rot}$, the post-shock temperature, T_2 is very close to the one predicted by CABARET. In Table 8, the data from the experiments is shown together with Tables 9 and 10 where the results from CABARET are exposed.

Testing conditions	**Post-shock temperature** [K]	**Total enthalpy** [MJ/kg]
FC-I	6100	16.5
FC-III	4600	10.1

Table 8: Post-shock temperatures and total enthalpies for FC-I and FC-III

N	**Scenario**	**Post-shock temperature** [K]	**Total enthalpy** [MJ/kg]
1	q_w,P_{t2},P_0	5767.55	14.1
2	q_w,P_0,T_0	5922.7	15.75
3	P_{t2},P_0,T_0	5981.026	15.74
4	q_w,$P_{t2}\dot{m}$	5767.83	14.02
5	q_w,T_0,$\dot{m}$	5923.71	15.76
6	q_w,P_0,$\dot{m}$	5947.0	16.05
7	P_{t2},T_0,$\dot{m}$	5982.44	15.76
8	P_{t2},P_0,$\dot{m}$	6016.24	16.06

Table 9: Post-shock temperatures and total enthalpies for FC-I

N	**Scenario**	**Post-shock temperature** [K]	**Total enthalpy** [MJ/kg]
1	q_w,P_{t2},P_0	3275.13	6
2	q_w,P_0,T_0	4446.56	9.47
3	P_{t2},P_0,T_0	4497.38	9.34
4	q_w,$P_{t2}\dot{m}$	3274.07	6
5	q_w,T_0,$\dot{m}$	4459.81	9.55
6	q_w,P_0,$\dot{m}$	4990.11	13.83
7	P_{t2},T_0,$\dot{m}$	4570.016	9.55
8	P_{t2},P_0,$\dot{m}$	5328.51	13.8

Table 10: Post-shock temperatures and total enthalpies for FC-III

As can be appreciated the results for FC-I are very close to the experimental data for both the post-shock temperature and the total enthalpy. For FC-III there are some rebuilding scenarios which work very well and other that show more distant results, this comes together with the highly dispersed results for the rebuilt free stream parameters. For high heat fluxes conditions such as FC-I and FC-II, the code works well because the convergence towards a supersonic solution is better.

3.3 Sensitivity analysis

The first step towards an uncertainty quantification study is to carry out a sensitivity analysis by propagating linearly the experimental uncertainties on the rebuilt parameters. The equations used for the computation of the sensitivity analysis are depicted below under the assumption that each contribution is independent to the global variability which can be expressed then as the norm of the different partial derivatives with their correspondent uncertainty:

$$\begin{aligned}
\Delta T_\infty &= \sqrt{\left(\frac{\partial T_\infty}{\partial x_1}\right)^2 (\Delta x_1)^2 + \left(\frac{\partial T_\infty}{\partial x_2}\right)^2 (\Delta x_2)^2 + \left(\frac{\partial T_\infty}{\partial x_3}\right)^2 (\Delta x_3)^2} \\
\Delta p_\infty &= \sqrt{\left(\frac{\partial p_\infty}{\partial x_1}\right)^2 (\Delta x_1)^2 + \left(\frac{\partial p_\infty}{\partial x_2}\right)^2 (\Delta x_2)^2 + \left(\frac{\partial p_\infty}{\partial x_3}\right)^2 (\Delta x_3)^2} \\
\Delta M_\infty &= \sqrt{\left(\frac{\partial M_\infty}{\partial x_1}\right)^2 (\Delta x_1)^2 + \left(\frac{\partial M_\infty}{\partial x_2}\right)^2 (\Delta x_2)^2 + \left(\frac{\partial M_\infty}{\partial x_3}\right)^2 (\Delta x_3)^2}
\end{aligned}$$

The variables x_1, x_2 and x_3 used here are the different parameters needed to do the rebuilding for the different scenarios. For the complete determination of the sensitivity analysis, the partial derivatives as well as the experimental uncertainties of the instruments need to be

known.

The contribution of each parameter to the total variability of the results can be computed once the experimental uncertainties are known. They are computed as the partial derivative multiplied by the experimental uncertainty. As can be appreciated in the following tables (Tables 11-13), the contributions are computed for the three different test cases:

FC-I test case	$(\partial T_\infty/\partial x_i)\Delta x_i$	$(\partial p_\infty/\partial x_i)\Delta x_i$	$(\partial M_\infty/\partial x_i)\Delta x_i$
$x_1 = q_w[W/m^2]$	155.2	912	-0.19
$x_2 = p_{t2}[Pa]$	10.46	64.68	-0.009
$x_3 = p_0[Pa]$	-4.45	-1.95	0.00457
$x_4 = T_0[K]$	535	-2247.15	0.054
$x_5 = \dot{m}[kg/s]$	-32.33	-21.7	0.012

Table 11: Contributions to error bars for the FC-I test case

FC-II test case	$(\partial T_\infty/\partial x_i)\Delta x_i$	$(\partial p_\infty/\partial x_i)\Delta x_i$	$(\partial M_\infty/\partial x_i)\Delta x_i$
$x_1 = q_w[W/m^2]$	92	3000.5	-0.144
$x_2 = p_{t2}[Pa]$	4.4	133.56	-0.007
$x_3 = p_0[Pa]$	-3.04	-24.19	0.00511
$x_4 = T_0[K]$	28.95	-4844.25	0.28
$x_5 = \dot{m}[kg/s]$	-1.27	-12.12	0.00213

Table 12: Contributions to error bars for the FC-II test case

FC-III test case	$(\partial T_\infty/\partial x_i)\Delta x_i$	$(\partial p_\infty/\partial x_i)\Delta x_i$	$(\partial M_\infty/\partial x_i)\Delta x_i$
$x_1 = q_w[W/m^2]$	102.176	25.42	-0.18
$x_2 = p_{t2}[Pa]$	2.7	4.15	-0.00567
$x_3 = p_0[Pa]$	14.22	-1.87	0.000144
$x_4 = T_0[K]$	252.45	-39.32	0.133
$x_5 = \dot{m}[kg/s]$	-7.06	0.58	-0.00494

Table 13: Contributions to error bars for the FC-III test case

Once all the information needed is known, the sensitivity analysis can be performed and the results are analyzed in Figs. 5-13 and Tables 14-16.

N	**Scenario**	$\Delta T_\infty/T_\infty$ [%]	$\Delta p_\infty/p_\infty$ [%]	$\Delta M_\infty/M_\infty$ [%]
1	q_w,P_{t2},P_0	4.6	20.93	5.6
2	q_w,P_0,T_0	16.0	76.6	5.68
3	P_{t2},P_0,T_0	14.52	50.36	1.7
4	q_w,P_{t2},$\dot{m}$	4.71	20.54	5.7
5	q_w,T_0,$\dot{m}$	16.01	76.6	5.7
6	q_w,P_0,$\dot{m}$	4.51	30.29	5.47
7	P_{t2},T_0,$\dot{m}$	14.51	50.17	1.73
8	P_{t2},P_0,$\dot{m}$	0.009	1.51	0.00487

Table 14: Sensitivity analysis for FC-I (relative error)

The results shown on Table 14 are plotted below in Figs. 5-7. As can be appreciated in Fig. 5, the rebuilding scenarios with the largest error bars are those involving the reservoir temperature (T_0) such as 2, 3, 5 and 7. This is due to the high level of uncertainty associated with this particular measurement in relation to the free stream temperature for this particular problem. This tendency can be also appreciated in the free stream pressure in Fig. 6. For the free stream Mach number, the main contribution is not the reservoir temperature but the heat flux. It can be observed in Fig.7 that the rebuilding scenarios with the largest uncertainties are the ones involving this measurement. Despite having a higher experimental uncertainty, the reservoir temperature does not contribute as much as the heat flux, this is due to the partial derivatives of the Mach number in relation with these two measurements which involves the nature of the problem itself.

The uncertainty associated with the rebuilding scenario 8 is relatively small in general for all the three cases. It is also important to notice that these levels of uncertainties in the sensitivity analysis are based on **strong assumptions** regarding the flow conditions and modeling. Epistemic uncertainties, related to the model used in CABARET, would play an important role as well but they are not taken into account for this study.

In Tables 15-16 and Figs. 8-13, the results of the sensitivity analysis performed under testing conditions FC-II and FC-III are depicted.

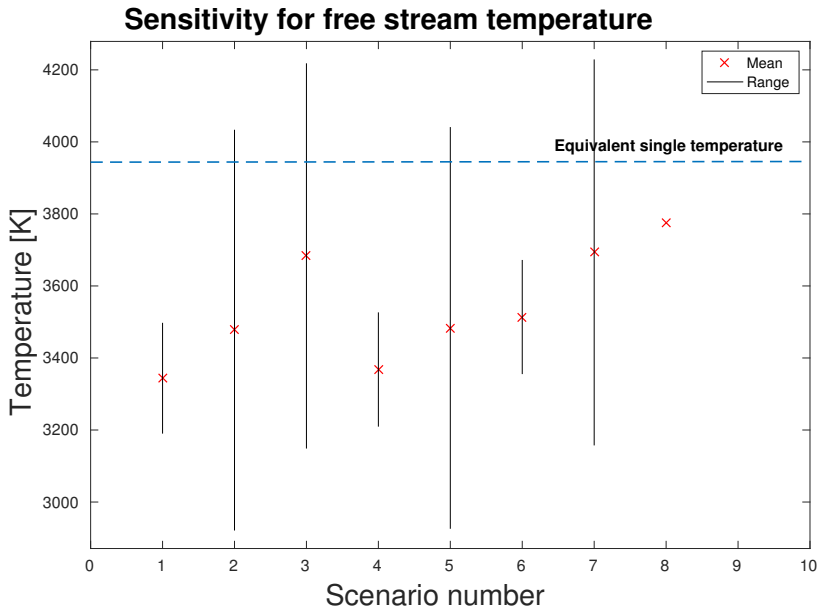

Figure 5: Sensitivity for the free stream temperature

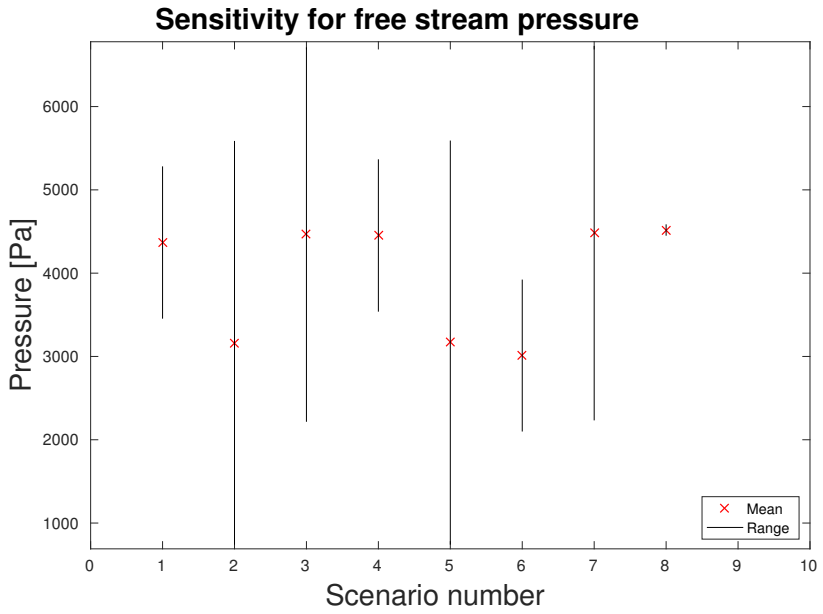

Figure 6: Sensitivity for the free stream pressure

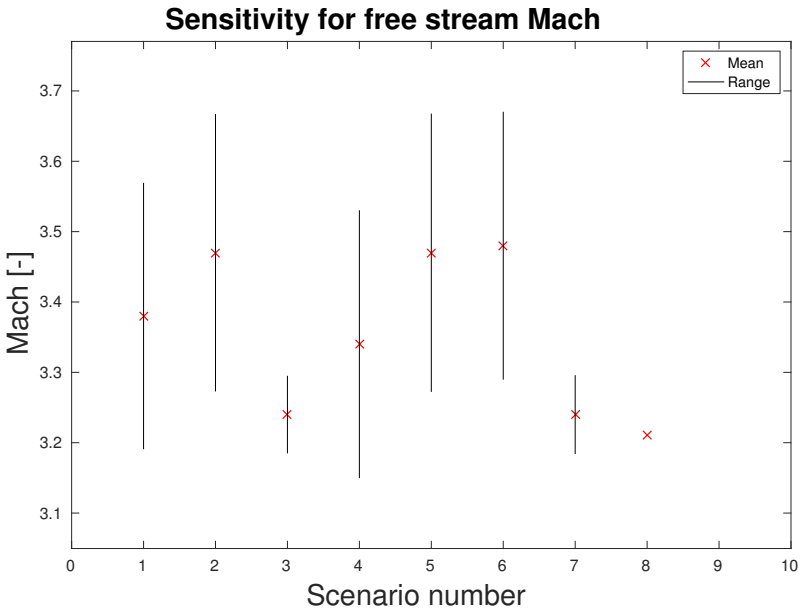

Figure 7: Sensitivity for the free stream Mach number

N	**Scenario**	$\Delta T_\infty/T_\infty$ [%]	$\Delta p_\infty/p_\infty$ [%]	$\Delta M_\infty/M_\infty$ [%]
1	q_w,P_{t2},P_0	2.93	31.42	4.53
2	q_w,P_0,T_0	3.07	55.6	10.12
3	P_{t2},P_0,T_0	0.944	50.4	8.83
4	q_w,P_{t2},$\dot{m}$	2.93	31.5	4.76
5	q_w,T_0,$\dot{m}$	3.0	55.48	10.0
6	q_w,P_0,$\dot{m}$	2.9	29.57	4.7
7	P_{t2},T_0,$\dot{m}$	0.939	50.31	8.86
8	P_{t2},P_0,$\dot{m}$	0.175	1.42	0.28

Table 15: Sensitivity analysis for FC-II (relative error)

When comparing the FC-II test case to the FC-I test case, one can notice that the level of uncertainty in the free stream pressure is significantly higher than both the free stream temperature and the Mach number. The largest contributions to this are when considering the heat flux and the reservoir temperature in the rebuilding scenario, such as scenarios 2 and 5 (see Figs. 8-10).

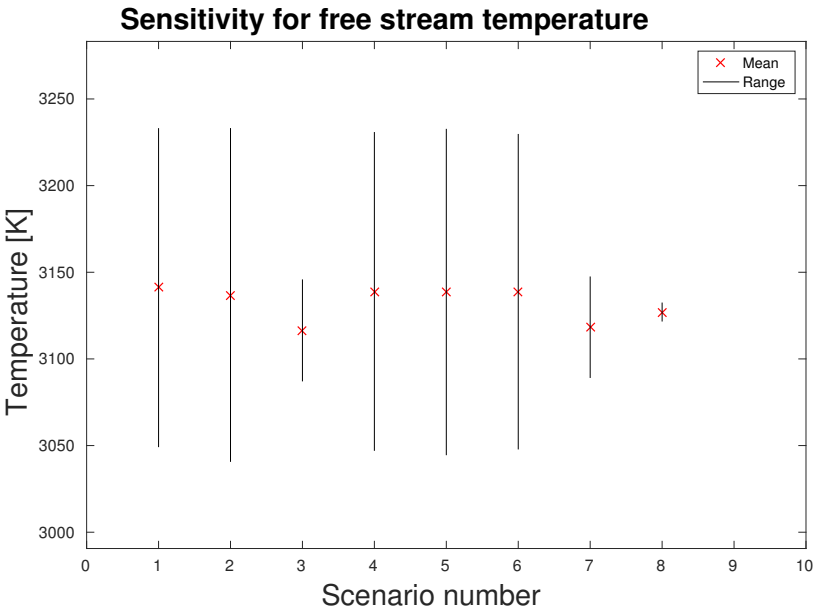

Figure 8: Sensitivity for the free stream temperature

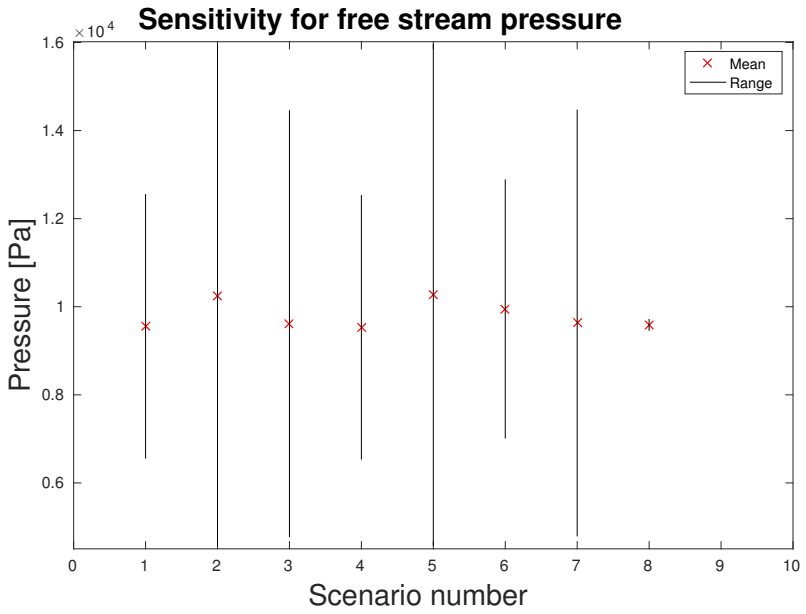

Figure 9: Sensitivity for the free stream pressure

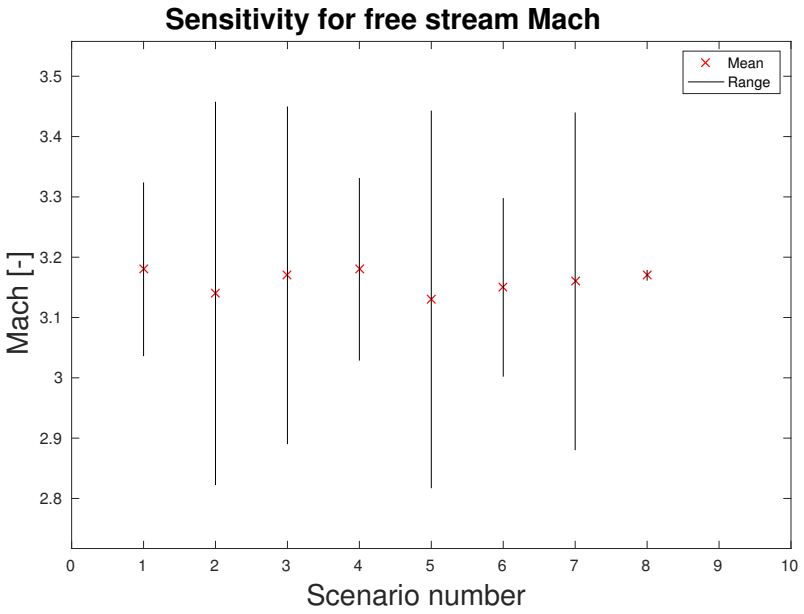

Figure 10: Sensitivity for the free stream Mach number

N	**Scenario**	$\Delta T_\infty/T_\infty$ [%]	$\Delta p_\infty/p_\infty$ [%]	$\Delta M_\infty/M_\infty$ [%]
1	q_w,P_{t2},P_0	10.57	11.11	3.39
2	q_w,P_0,T_0	18.1	54.95	4.16
3	P_{t2},P_0,T_0	12.87	12.52	2.88
4	q_w,P_{t2},$\dot{m}$	9.18	9.45	3.66
5	q_w,T_0,$\dot{m}$	16.82	51.21	4.31
6	q_w,P_0,$\dot{m}$	4.97	65.23	3.12
7	P_{t2},T_0,$\dot{m}$	12	11.0	3.35
8	P_{t2},P_0,$\dot{m}$	0.635	1.38	0.34

Table 16: Sensitivity analysis for FC-III (relative error)

Due to the low heat flux condition for the FC-III test case, the rebuilding results are more dispersed but the general tendency for the sensitivity analysis mentioned before is kept the same. The combination of heat flux and reservoir temperature generates the largest uncertainties and when comparing the three free stream parameters, the pressure is always the most affected by the experimental uncertainties as can be appreciated.

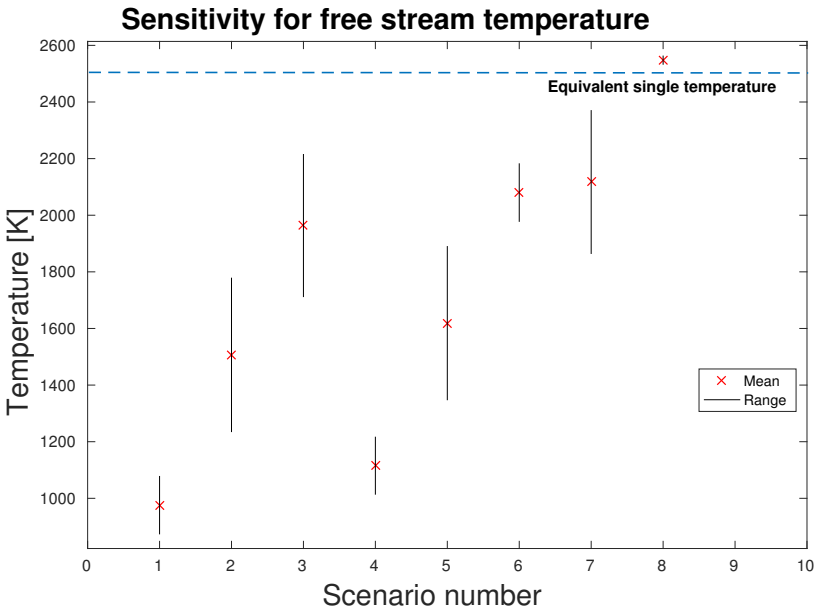

Figure 11: Sensitivity for the free stream temperature

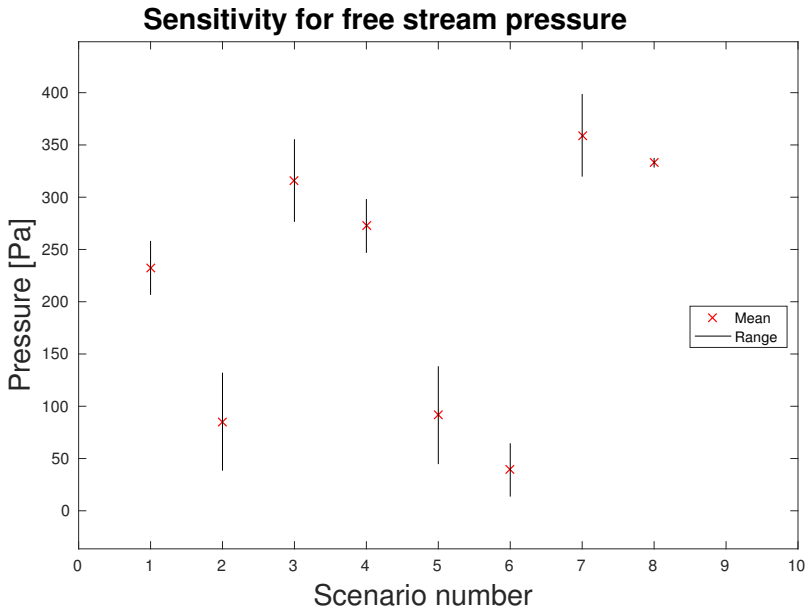

Figure 12: Sensitivity for the free stream pressure

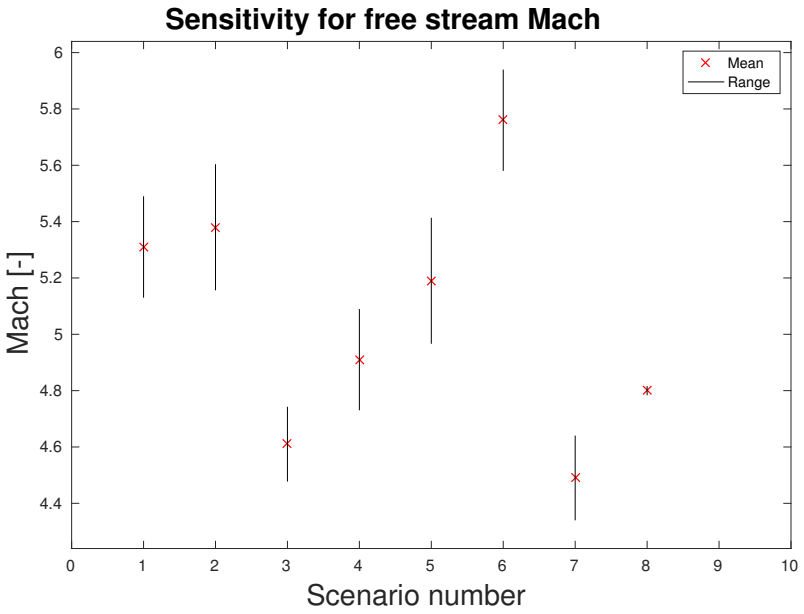

Figure 13: Sensitivity for the free stream Mach number

3.4 Uncertainty analysis

Uncertainty quantification studies provide more information about the parameters variability in terms of probability density functions than sensitivity analysis where just a linear variation of the uncertain parameters is taken into account. The Probability Density Functions (PDFs) of the free stream parameters are computed by this mean.

To be able to perform an uncertainty analysis with the different rebuilding scenarios, the uncertainty associated to the instruments used to measure the different inputs for CABARET needs to be known and characterized as a PDF itself for some sampling analysis, such as Monte Carlo. In this term, a Gaussian probability distribution function is assumed for our inputs for which the information of the instrumental uncertainties is essential.

Taking into account the computational cost involved in UQ analysis and the different rebuilding scenarios together with the three different test cases, a full UQ study was performed for the FC-II testing conditions with the stagnation pressure, reservoir pressure and mass flow measurements involved for scenarios 1 and 8.

Another variable to take into account in this study is the number of samples needed to have a representative statistical study of the problem. In the following graphs, the convergence of the mean value of the free stream parameters can be appreciated for an increasing number of samples (up to 5500).

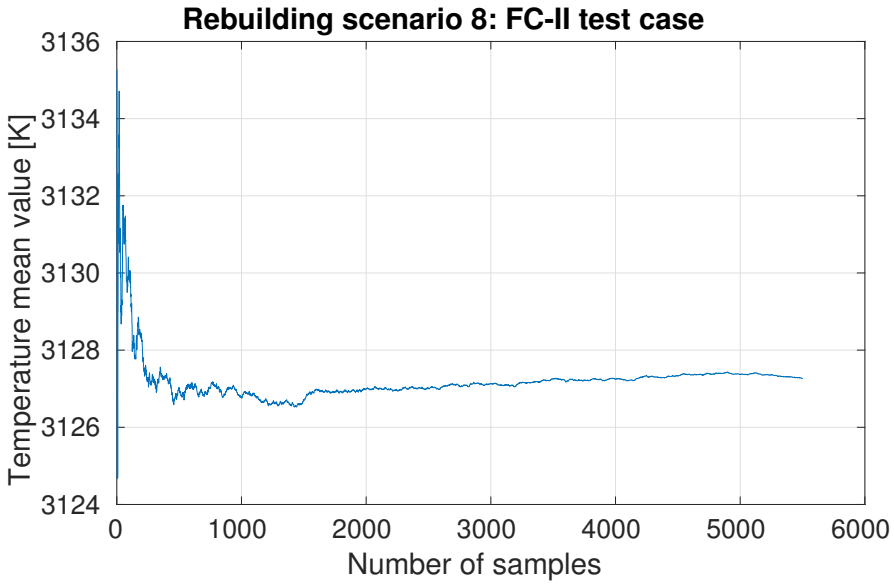

Figure 14: Evolution of the temperature mean value with the number of samples

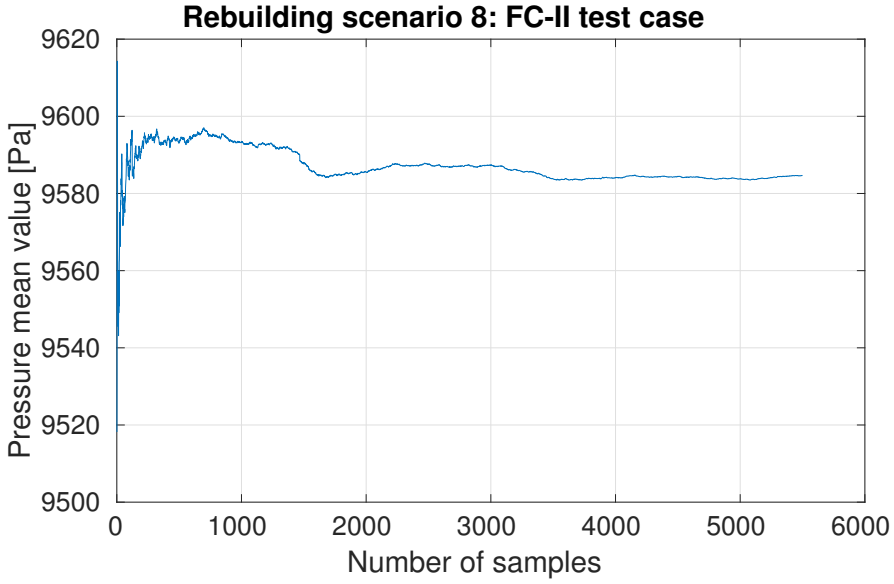

Figure 15: Evolution of the pressure mean value with the number of samples

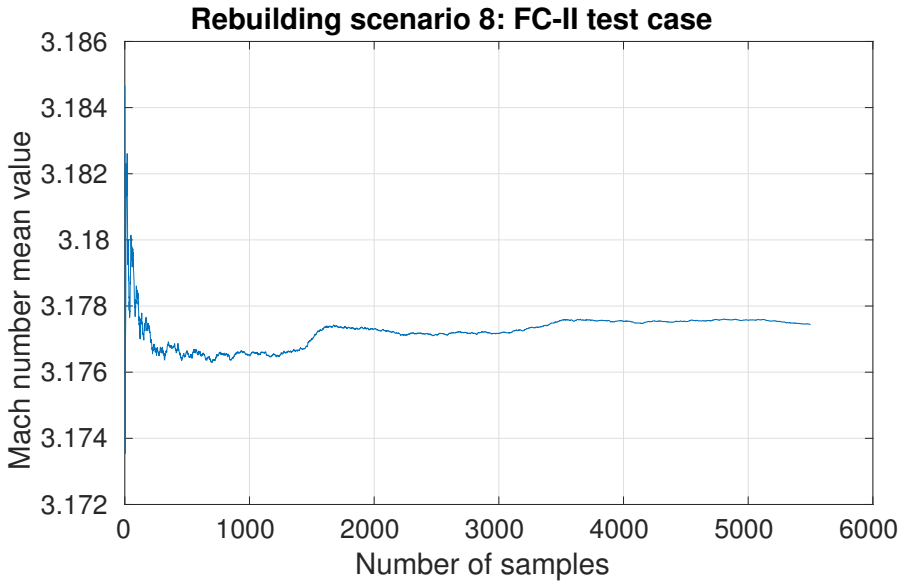

Figure 16: Evolution of the Mach number mean value with the number of samples

The UQ analysis was then performed for a number of samples of 100, 1000 and 5000 for scenario 8 as a comparative study, and 5000 for scenario 1. Some important differences between them can be appreciated in Figs. 17-19 as suggested by the convergence plots for the three parameters:

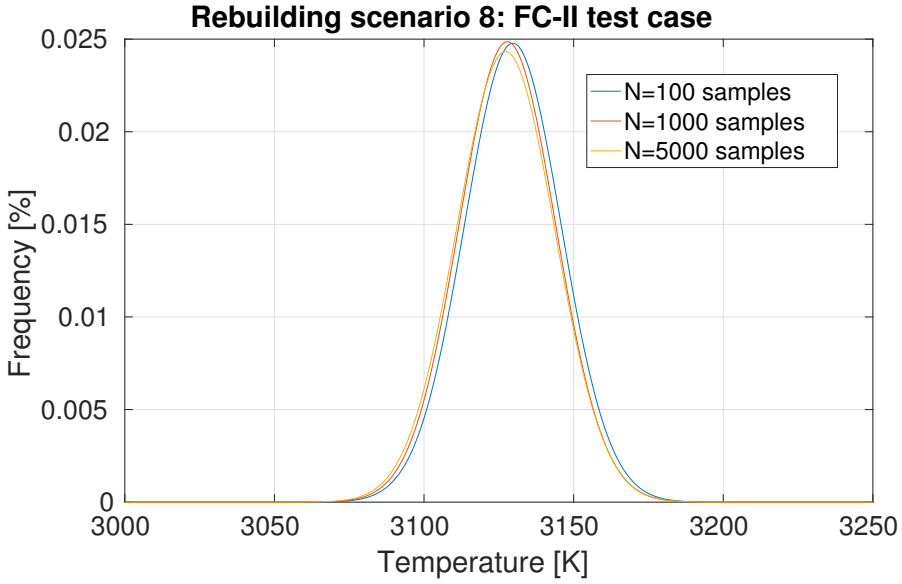

Figure 17: PDF of the rebuilt free stream temperature

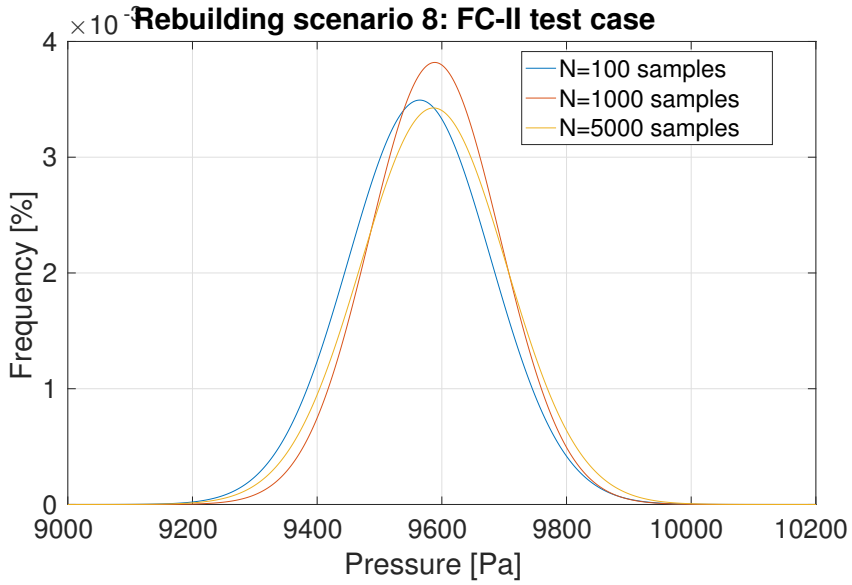

Figure 18: PDF of the rebuilt free stream pressure

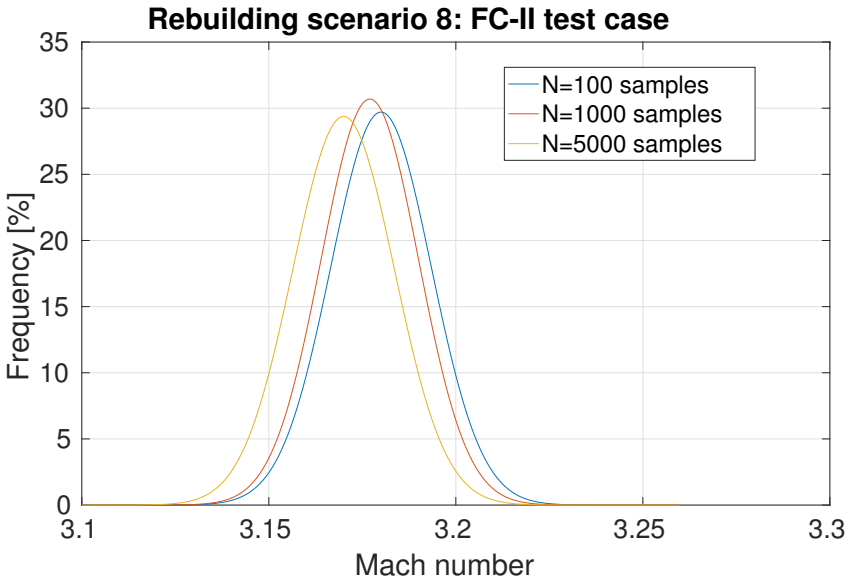

Figure 19: PDF of the rebuilt free stream Mach number

In Tables 17 and 18, the parameters of the PDFs are depicted. On these tables, the parameter *cov* from the UQ analysis is known as the coefficient of variation and it is expressed as:

$$cov = \frac{\sigma}{\mu} \tag{38}$$

This parameter shows the extent of variability in relation to the mean of the population.

PDF parameters	100 samples	1000 samples	5000 samples	**Sensitivity analysis**
μ_{T_∞} [K]	3129.67	3127.85	3127.26	3127.05
σ_{T_∞} [K]	16.1	16.057	16.4	5.47
cov_{T_∞}	0.00514	0.00513	0.00524	0.00175
μ_{p_∞} [Pa]	9564.55	9588.66	9586.66	9589
σ_{p_∞} [Pa]	114.2	104.47	116.46	136
cov_{p_∞}	0.012	0.01	0.012	0.0142
μ_{M_∞}	3.18	3.177	3.17	3.17
σ_{M_∞}	0.0134	0.013	0.0135	0.008876
cov_{M_∞}	0.00421	0.0041	0.00425	0.0028

Table 17: Probability Distribution Functions parameters for scenario 8

PDF parameters	5000 samples	**Sensitivity analysis**
μ_{T_∞} [K]	3133.2	3141.13
σ_{T_∞} [K]	100	92
cov_{T_∞}	0.032	0.029
μ_{p_∞} [Pa]	9533.4	9556.89
σ_{p_∞} [Pa]	2803.5	3002.7
cov_{p_∞}	0.294	0.3141
μ_{M_∞}	3.18	3.18
σ_{M_∞}	0.1366	0.144
cov_{M_∞}	0.043	0.045

Table 18: Probability Distribution Functions parameters for scenario 1

Taking a look back to the rebuilding results, one can compare the nominal conditions retrieved then and compare them to the uncertainty analysis results. The convergence of the mean values as shown in Figs. 14-16 towards the nominal values can be appreciated when compared to Table 19.

T_∞	3127.05
p_∞	9589.11
M_∞	3.17

Table 19: Nominal conditions under scenario 8

The variability computed by means of UQ and sensitivity analysis together with the coefficient of variation does not agree for scenario 8 as can be seen in Table 17 while for scenario 1, the variables are comparable in order of magnitude.

In order to study the influence of the uncertainty of each experimental variable on the determination of the free stream condition uncertainties, this is, how important is the variance of a particular input in the computation of the output's variance, the Sobol indices are computed from the UQ study:

$$S_i = \frac{V_i}{Var[Y]} \tag{39}$$

Being S_i the Main Sobol index for the variable i and V_i the variance of the same variable.

For rebuilding scenarios 1 and 8, the Main and Total indices are expressed in Tables 20-23.

Main Sobol indices	p_{t2}	p_0	$\dot{m}$
T_∞	0.0326	0.845	0.0363
p_∞	0.229	0.358	0.0423
M_∞	0.0419	0.76	0.026

Table 20: Main Sobol indices for scenario 8

Total Sobol indices	p_{t2}	p_0	$\dot{m}$
T_∞	0.053838	0.89291	0.092883
p_∞	0.60473	0.75517	0.5089
M_∞	0.1522	0.9036	0.1431

Table 21: Total Sobol indices for scenario 8

Main Sobol indices	q_w	p_{t2}	p_0
T_∞	0.9	0.018	0.009
p_∞	0.88	0.0013	0.000062
M_∞	0.93	0.002	0.0008

Table 22: Main Sobol indices for scenario 1

Total Sobol indices	q_w	p_{t2}	p_0
T_∞	0.95	0.0022	0.013
p_∞	0.9	0.0018	0.000066
M_∞	0.965	0.003	0.001

Table 23: Total Sobol indices for scenario 1

From these indices, the relative influence of the uncertainties of the experimental parameters can be extracted and compared to the results from the sensitivity analysis.

When looking at the Main Sobol indices, the largest one corresponds to the most influential parameter. Taking a look at Table 20, p_0 is the most influential parameter for the three free stream conditions while the sensitivity analysis predicts that p_{t2} plays this role for this rebuilding scenario as seen in Table 24. The same logic is applied to the rebuilding scenario 1, in which Table 22 and Table 25 agree on the most influential parameter.

Sensitivity analysis	p_{t2}	p_0	$\dot{m}$
T_∞	0.68	0.3	0.05
p_∞	0.96	0.03	0.0079
M_∞	0.61	0.33	0.057

Table 24: Relative influence of the parameters to the error bars for scenario 8

Sensitivity analysis	q_w	p_{t2}	p_0
T_∞	0.996	0.023	0.011
p_∞	0.998	0.002	0.0000648
M_∞	0.9964	0.0024	0.0013

Table 25: Relative influence of the parameters to the error bars for scenario 1

The Main Sobol indices also account for non-linearities between the parameters. In order to identify their possible presence, this index can be compared to the relative influence of the parameters when computing the sensitivity analysis which assumes the relations between the parameters to be linear.

As can be noted, the sensitivity analysis results do not correspond with the Main Sobol indices for scenario 8, therefore, non-linear effects have to be taken into account for this particular scenario. In the case of scenario 1, the Main Sobol Indices and the sensitivity analysis results shown in Table 25 are comparable in order of magnitude. For scenario 1 then, one can conclude that non-linear effects are not important when rebuilding using the heat flux, the stagnation and reservoir pressure.

The Total Sobol index also determines if there are cross-correlations between parameters. They have to be compared to the Main ones in order to determine whether there are cross-correlations or not. In the case of scenario 8, differences can be appreciated between both indices so one can safely conclude that cross-correlations are important. For scenario 1, on the other hand, cross-correlations are not important and a sensitivity analysis would be enough in order to have a reliable estimation of the uncertainties involved on this particular rebuilding.

4 Conclusions

The rebuilding of the free stream conditions under LTE assumptions for the DLR's LBK arc-jet facility has been done for three different testing conditions. Due to the versatility of this particular facility in terms of the experimental data available, different rebuilding scenarios have been defined and studied in the framework of sensitivity analysis.

Many differences can be found among the different scenarios in terms of rebuilding accuracy or error bars propagated through the problem from the experimental data. The strong assumptions under which the CABARET code works have to be taken into account when analyzing which scenarios are the best for rebuilding the free stream conditions.

Finally, an uncertainty quantification study was carried out for the FC-II test case and rebuilding scenarios 1 and 8 with different number of samples. The convergence plots show that with 5000 samples the mean values of the free stream parameters reach a steady solution so there is no need to go for more samples.

For scenario 1, the comparison between the UQ results and the nominal conditions retrieved from the deterministic problem of the rebuilding shows good agreement between them. The agreement is kept also when comparing the Sobol indices to the values of the contribution of each parameter on Table 25.

In the case of scenario 8, the comparison between the Sobol indices and the values of the contribution of each parameter on Table 24 does not show the same results, being the reservoir pressure the most influential parameter for the free stream conditions according to the UQ study and the stagnation pressure according to the sensitivity analysis. Regarding the nominal conditions, they moatch in both UQ study and sensitivity analysis.

The interpretation of these results could lead to state that non-linearities are present in this particular rebuilding scenario in terms of how the inputs and outputs are related. In this case, the uncertainty quantification study would be necessary in order to characterize better the variability intervals of the free stream parameters rebuilt.

A The Fay-Riddell equation

A.1 General expression and assumptions

The Fay-Riddell equation is widely used to relate the stagnation point heat flux to the free stream total enthalpy. It has been derived by Fay and Riddell (1958) based on the following assumptions/restrictions:

- the boundary layer is laminar at the stagnation point,
- the boundary layer thickness is small with respect to the nose curvature radius which ensures that all the incoming flow has passed through a normal shock wave,
- the flow is in local thermodynamic and chemical equilibrium at the edge of the boundary layer,
- radiation heat flux is neglected,
- the shock layer can be partially dissociated and be of binary mixture type, i.e. made from molecules and atoms of similar molecular weight and collision cross section (typically N_2 and O_2 in air),
- the chemical reactions in the boundary layer in the vicinity of the stagnation point can be in equilibrium, non-equilibrium or frozen depending on τ_f and τ_c (flow characteristic time and rate of chemical reactions),
- the wall can be catalytic,
- and the velocity distribution at the outer edge of the boundary layer follows expressions obtained from incompressible flows.

Starting from boundary layer equations for global continuity, species continuity, momentum and energy, Fay and Riddell have obtained a set of nonlinear ordinary differential equations for the stagnation point. These self-similar solutions hold for chemically reacting viscous flows.

As explained in the main document, the original Fay-Riddell equation for a hemispherical probe is expressed as follows:

$$q_w = 0.763 Pr^{-0.6} (\rho_w \mu_w)^{0.1} (\rho_e \mu_e)^{0.4} (H_e - H_w) \sqrt{\beta_e} \left[1 + (Le^{0.52} - 1) \frac{h_D}{H_2} \right] \tag{40}$$

All the symbols and subscripts are detailed in Fay and Riddell (1958).

As noted in their paper, external flow properties are more important than the ones at the wall and the uncertainty in the predicted heat transfer is about 40% of the uncertainty

in the external viscosity. Experimental results have reported 10 to 20% deviations from the predictions (Holden (1985)). It is nevertheless generally agreed that the Fay-Riddell equation is accurate for engineering purposes (Lewis and Burgess III (1963)).

A.2 Velocity gradient at the stagnation point

The Fay-Riddell equation strongly depends upon the velocity gradient at the stagnation point, which has the second highest exponent in this expression. This parameter can be expressed differently depending on the assumptions made. Summarizing Olivier (1993) and Olivier (1995), different options exist:

- using the Newtonian theory. The flow velocity component which is normal to the surface is converted into pressure while the tangential component is conserved. Considering streamlines in the vicinity of the stagnation point, the stagnation point velocity gradient is given as (Olivier (1993)):

$$\left(\frac{\partial u}{\partial y}\right)_s = \frac{u_\infty}{R_{eff}} \tag{41}$$

  It is a crude approximation and better expressions should be preferred.

- using a one-dimensional momentum equation and assuming a Newtonian pressure distribution over the model (derived by Linnell (1957), and used by Fay and Riddell). In addition, the flow is assumed to be of constant density through the shock layer in the vicinity of the stagnation point (this is reasonably accurate for hypersonic flows). This leads to:

$$\left(\frac{\partial u}{\partial y}\right)_s = \frac{u_\infty}{R_{eff}}\sqrt{\frac{\rho_2}{\rho_{t2}}k(2-k)} \tag{42}$$

  where $k = \rho_1/\rho_2$ is the inverse of the shock density ratio. This expression therefore accounts for the ratio of density across the shock which depends on M_1. This can also be written as follows using the Newtonian pressure distribution assumption:

$$\left(\frac{\partial u}{\partial y}\right)_s = \frac{1}{R_{eff}}\sqrt{\frac{2(p_s - p_\infty)}{\rho_s}} \tag{43}$$

  The influence of the shock stand-off distance and of the vorticity produced by the curved shock are neglected. In wind tunnels with perfect gas conditions, the velocity gradient seems to be well approximated by eq. 42 (Curtiss and Boison (1959); Olivier (1995)).

- using a potential flow solution derived by Stokes and reported by Olivier (1993, 1995). Considering two concentric spheres (one for the probe and one for the shock wave around it), the velocity gradient is then expressed as:

$$\left(\frac{\partial u}{\partial y}\right)_s = \frac{u_2}{R_{eff}} \left[1 + \frac{1 + \frac{(1+\bar{\Delta})^3}{2}}{(1+\bar{\Delta})^3 - 1}\right] \tag{44}$$

where $\bar{\Delta} = \Delta / R_{eff}$ is the dimensionless shock stand-off distance. This expression (introduced by Olivier and Grönig (1993)) assumes an incompressible irrotational flow between the two spheres which is a very good approximation along the stagnation line for low temperatures or equilibrium flows. Expressions for the shock stand-off distance can be found in Olivier (1995).

- using an integral method (Olivier (1995)). This includes vorticity, compressibility and high-temperature gas effects. The velocity gradient is:

$$\left(\frac{\partial u}{\partial y}\right)_s = \frac{u_\infty}{R_{eff}} \frac{1+\bar{\Delta}}{\bar{\Delta}} \frac{p_s - p_2}{\rho_\infty u_\infty^2} \frac{\rho_2}{\rho_s} \tag{45}$$

This method seems better suited in the event of high temperature effects since chemistry allows for larger density ratio across the shock wave ($\rho_2/\rho_1 > 6$ unlike the theoretical limit reached for perfect gases), thus reducing $\bar{\Delta}$ and increasing the corresponding velocity gradient.

In all the previous expressions, it is evident that $(\partial u/\partial y)_s \propto 1/R_{eff}$. Hence, inserting it into eq. 39, the stagnation point heat flux q_w is inversely proportional to the square root of the nosetip radius $R_{eff} (q_w \propto 1/\sqrt{R_{eff}})$. This is a well established result for hypersonic flows (Allen and Eggers (1953)) which has lead to the successful blunt shape of the early hypersonic re-entry vehicles (Vostok, Mercury, Gemini, Apollo...) minimizing the stagnation point heat transfer.

A.3 Other equations estimating the stagnation point heat flux

Alternatives to the Fay-Riddell equation exist such as the ones from Sibulkin (1952); van Driest (1956); Kemp and Riddell (1957); Detra et al. (1957). Extension to gases different from air and some mixtures have been performed respectively by Zoby (1968) and Sutton and Graves (1971).
More recently, Sargnier and Vérant (1998a) and Sargnier and Vérant (1998b) performed numerical computations on a hemispherical probe assuming a catalytic wall and a perfect gas flow. They correlated their results at the stagnation point as:

$$q_w = 23.79 \left[\frac{h_0 - h_w}{r T_{ref}}\right]^{1.069} \sqrt{\frac{p_{t2}}{R_{eff}}} \tag{46}$$

with $T_{ref} = 273.15K$.

Constants were found using a least square method. Results have an uncertainty about ± 12%. The main interest of such an equation is that it does not require the knowledge of any free stream property.

B Relative contribution of the experimental data to the free stream parameters

N	Scenarios	T_∞	p_∞	M_∞
1	q_w,p_{t2},p_0	99.46,0.451,0.0817	99.49,0.5,0.000454	99.71,0.22,0.00577
2	q_w,p_0,T_0	7.76,0.00638,92.23	14.14,0.00006.46,85.85	92.47,0.0535,7.47
3	p_{t2},p_0,T_0	0.0382,0.0069,99.95	0.082,0.000075,99.9	2.68,0.69,96.6
4	q_w,p_{t2},$\dot{m}$	95.43,0.43,4.14	99.44,0.5,0.05	99.38,0.22,0.4
5	q_w,T_0,$\dot{m}$	7.74,91.93,0.34	14.14,85.85,0.008	92.19,7.45,0.37
6	q_w,p_0,$\dot{m}$	95.77,0.0787,4.16	99.94,0.00045,0.0565	99.55,0.0575,0.4
7	p_{t2},T_0,$\dot{m}$	0.038,99.6,0.36	0.0827,99.91,0.0093	2.58,92.84,4.58
8	p_{t2},p_0,$\dot{m}$	9.32,1.69,89.0	89.81,0.0816,10.11	32.94,8.49,58.56

Table 26: Contributions to the error bars for FC-I test case

N	Scenarios	T_∞	p_∞	M_∞
1	q_w,p_{t2},p_0	99.66,0.23,0.11	99.8,0.2,0.00648	99.64,0.24,0.13
2	q_w,p_0,T_0	90.9,0.099,9.0	27.73,0.0018,72.27	20.91,0.0263,79.06
3	p_{t2},p_0,T_0	2.23,1.07,96.7	0.0759,0.00249,99.92	0.06244,0.03327,99.9
4	q_w,p_{t2},$\dot{m}$	99.75,0.23,0.019	99.8,0.2,0.00162	99.74,0.24,0.0218
5	q_w,T_0,$\dot{m}$	90.97,9.01,0.0173	27.73,72.27,0.00045	20.92,79.08,0.00457
6	q_w,p_0,$\dot{m}$	99.87,0.11,0.019	99.99,0.00649,0.0016	99.85,0.13,0.0218
7	p_{t2},T_0,$\dot{m}$	2.25,97.56,0.19	0.0759,99.92,0.000625	0.0624,99.93,0.00578
8	p_{t2},p_0,$\dot{m}$	68.08,30.59,5.34	96.06,3.15,0.79	61.52,32.78,5.7

Table 27: Contributions to the error bars for FC-II test case

N	Scenarios	T_∞	p_∞	M_∞
1	q_w,p_{t2},p_0	98.03,0.068,1.9	96.89,2.58,0.52	99.9,0.099,0.000063
2	q_w,p_0,T_0	14.04,0.27,85.69	29.43,0.16,70.41	64.68,0.0000413,35.32
3	p_{t2},p_0,T_0	0.011,0.32,99.67	1.1,0.22,98.68	0.18,0.00011,99.82
4	q_w,p_{t2},$\dot{m}$	99.46,0.069,0.47	97.35,2.59,0.05	99.83,0.099,0.075
5	q_w,T_0,$\dot{m}$	14.07,85.87,0.067	29.47,70.51,0.015	64.65,35.3,0.0486
6	q_w,p_0,$\dot{m}$	97.64,1.89,0.47	99.41,0.54,0.051	99.92,0.000064,0.0752
7	p_{t2},T_0,$\dot{m}$	0.011,99.91,0.078	1.1,98.88,0.0215	0.18,99.68,0.14
8	p_{t2},p_0,$\dot{m}$	2.81,77.97,19.22	81.79,16.61,1.6	56.83,0.036,43.14

Table 28: Contributions to the error bars for FC-III test case

References

Allen, H.J. and Eggers, Jr, A.J. (1953). *A study of the motion and aerodynamic heating of missiles entering the Earth's atmosphere at high supersonic speeds.* Research Memorandum NACA RM A53D28, National Advisory Committee for Aeronautics.

Anderson Jr, J.D. (2006). *Hypersonic and High-Temperature Gas Dynamics. Second Edition.* AIAA Education Series.

Barker, M. (1922). *On the Use of Very Small Pitot-Tubes for Measuring Wind Velocity.* Proc. R. Soc. London, 1922.

Bottin, B., Chazot, O., Carbonaro, M., Van Der Haegen, V. & Paris, S. (1999). *The VKI Plasmatron Characteristics and Performance.* Educational Notes RTO-EN-AVT-008, RTO, 1999.

Curtiss, H. A. & Boison, J. C. (1959). *An Experimental Investigation of Blunt Body Stagnation Point Velocity Gradient.* ARS Journal, February 1959.

Detra, R.W., Kemp, N.H. and Riddell, F.R. (1957). *Addendum to heat transfer to satellite vehicles reentering the atmosphere.* Jet Propulsion, 27(12): pp. 1256-1257.

Fay, J.A. & Riddell, F.R. (1958). *Theory of Stagnation Point Heat Transfer in Dissociated Air.* Journal of the Aeronautical Sciences, pages 73-85, February 1958.

Goulard, R. (1958). *On Catalytic Recombination Rates in Hypersonic Stagnation Heat Transfer.* ARS 12th Annual Meeting, New York, USA, July 1958.

Gülhan, A. & Esser, B. (2002). *Arc-Heated Facilities as a Tool to Study Aerothermodynamic Problems of Reentry Vehicles.* Lu, F.K.; Marren, D.E. (Eds): Advanced Hypersonic Test Facilities, Progress in Astronautics and Aeronautics, Vol. 198, pp. 375-403. AIAA, 2002.

Gülhan, A., Esser, B., Koch, U. & Hannemann, H. (2001). *Mars Entry Simulation in the Arc-Heated Facility L2K.* 4th European Symposium on Aerothermodynamics of Space Vehicles, Capua, Italy, October 2001.

Holden, M.S. (1985). *Studies for potential fluid-mechanical mechanisms for enhanced stagnation-region heating.* 20th AIAA Thermophysics conference, AIAA 1985-1002.

Kemp, N.H. and Riddell, F.R. (1957). *Heat transfer to satellite vehicles re-entering the atmosphere.* Jet Propulsion, 27(2): pp. 132-137.

Le Quang Huy, D. (2014). *Spectroscopic measurements of sub- and supersonic plasma flows for the investigation of atmospheric re-entry shock layer radiation.* Ph.D Thesis, von Karman Institute for Fluid Dynamics-Université Blaise Pascal.

Lewis, C.H. and Burgess III, E.G. (1963). *Charts of sphere stagnation heat-transfer rate in air and nitrogen at high temperatures.* Tech. Rep. AEDC-TDR-63-139, Arnold Engineering Development Center.

Linnell, R.D. (1957). *Incompressible Newtonian hypersonic flow around a sphere.* Research Note 5, Convair Scientific Research Laboratory.

Olivier, H. (1993). *An improved method to determine free stream conditions in hypersonic facilities.* Shock Waves, 3(3): pp. 129-139.

Olivier, H. (1995). *Influence of the velocity gradient on the stagnation point heating in hypersonic flow.* Shock Waves, 5(4): pp. 205-216.

Olivier, H. and Grönig, H. (1993). *Hypersonic model testing in a shock tunnel.* 5th AIAA international aerospace and hypersonics technologies conference, AIAA paper 1993-5004.

Sargnier, P. and Vérant, J.L. (1998a). *Flow characterization in the ONERA F4 high-enthalpy wind tunnel.* AIAA Journal, 36(4): pp. 522-532.

Sargnier, P. and Vérant, J.L. (1998b). *On the validation of high enthalpy wind tunnel simulations.* Aerospace Science and Technology, 2(7): pp. 425-437.

Scoggins, J.B. & Magin, T.E. (2014). *Development of MUTATION++: MUlticomponent Thermodynamics And Transport properties for IONized gases library in C++.* 11th AIAA/ASME Joint Thermophysics and Heat Transfer Conference, Atlanta, USA, June 2014.

Sibulkin, M. (1952). *Heat transfer near the forward stagnation point of a body of revolution.* Journal of Aeronautical Sciences, 19(8): pp. 570-571.

Sutton, K.S. and Graves, Jr, R.A.(1971). *A general stagnation-point convective-heating equation for arbitrary gas mixtures.* Technical report NASA TR R-376, NASA.

Van Der Haegen, V. (2013). *Development of an All-Speed Approximate Riemann Solver Applied to Supersonic Plasmas.* VKI PR, von Karman Institute for Fluid Dynamics, Rhode-St-Genèse, Belgium, June 2013.

van Driest, E.R. (1956). *The problem of aerodynamic heating.* Aeronautical Engineering Review, 15(10): pp. 26-41.

Zoby, E.V. (1968). *Empirical stagnation-point heat-transfer relation in several gas mixtures at high enthalpy levels.* Technical Note NASA TN D-4799, Langey Research Center.